



City Research Online

## City, University of London Institutional Repository

---

**Citation:** Geber, E., Rodriguez, C., Karathanassis, I. K., Lopez-Pintor, D., Manin, J., Pickett, L. & Gavaises, M. (2023). A general predictive methodology for fuel-mixture properties up to supercritical conditions. *Fluid Phase Equilibria*, 574, 113888. doi: 10.1016/j.fluid.2023.113888

This is the published version of the paper.

This version of the publication may differ from the final published version.

---

**Permanent repository link:** <https://openaccess.city.ac.uk/id/eprint/30980/>

**Link to published version:** <https://doi.org/10.1016/j.fluid.2023.113888>

**Copyright:** City Research Online aims to make research outputs of City, University of London available to a wider audience. Copyright and Moral Rights remain with the author(s) and/or copyright holders. URLs from City Research Online may be freely distributed and linked to.

**Reuse:** Copies of full items can be used for personal research or study, educational, or not-for-profit purposes without prior permission or charge. Provided that the authors, title and full bibliographic details are credited, a hyperlink and/or URL is given for the original metadata page and the content is not changed in any way.

---

City Research Online:

<http://openaccess.city.ac.uk/>

[publications@city.ac.uk](mailto:publications@city.ac.uk)

---



# A general predictive methodology for fuel-mixture properties up to supercritical conditions

E. Geber<sup>a,\*</sup>, C. Rodriguez<sup>a,b</sup>, I.K. Karathanassis<sup>a</sup>, D. Lopez-Pintor<sup>b</sup>, J. Manin<sup>b</sup>, L. Pickett<sup>b</sup>, M. Gavaises<sup>a</sup>

<sup>a</sup> School of Science & Technology, City, University of London, Northampton Square, EC1V 0HB London, United Kingdom

<sup>b</sup> Combustion Research Facility, Sandia National Laboratories, 7011 East Ave, Livermore, CA 94550, United States

## ARTICLE INFO

### Keywords:

PC-SAFT

Vapor-liquid equilibrium

Fuel surrogates

Multicomponent fuels

Group contribution theory

## ABSTRACT

A predictive thermodynamic model is utilized for the calculation of fuel properties of oxymethylene dimethyl ethers (OME<sub>3-4</sub>), surrogates for gasoline, diesel and aviation fuel, as well as alcohol blends with gasoline and diesel. The alcohols used for these blends are methanol, ethanol, propanol, butanol and pentanol; their mixing ratio ranges from 10 to 50% by volume. The model is based on the Perturbed-Chain Statistical Association Fluid Theory (PC-SAFT) equation of state (EoS) and Vapor Liquid Equilibrium (VLE) calculations at constant temperature, density and composition. The model includes the association term, with the assumption of two association sites (2B scheme), to enable the modeling of alcohols. The pure-component parameters are estimated based on the Group Contribution (GC) method of various sources, as well as a parametrization model specifically designed for the case of OME<sub>3-4</sub>. The results of the computational model for the density, vapor pressure and distillation curves at various conditions, including high-pressure, high-temperature (HPHT), are compared to experimental and computational data available in the literature. In the cases where no measurements are available for the surrogates, experimental data for the corresponding target fuel are used, taking into consideration the inherent deviation in properties between real and surrogate fuel. Overall, the results are in good agreement with the data from the literature, with the average deviation not exceeding 12% for temperature (Kelvin) on the distillation curves, 10% for density and 46% for vapor pressure and the general trend being captured successfully. The use of different pure component parameter estimation techniques can further improve the prediction quality in the cases of OME<sub>3-4</sub> and the aviation fuel surrogate, especially for the vapor pressure, leading to an average deviation lower than 18%. These results demonstrate the predictive capabilities of the model, which extend to a wide range of fuel types and pressure/temperature conditions. Through this investigation, the present work aims to establish the limits of applicability of this thermodynamic property prediction methodology.

## 1. Introduction

While electrification is often proposed as a solution to reduce CO<sub>2</sub> emissions from passenger cars, it seems unlikely that this can be the case for heavy-duty, marine and aviation powertrains. The European Commission, in the Future Transport Fuels report [1], suggests that only passenger cars, road freight transport and rail will be able to rely on electric energy and mostly for short to medium distances. This means that in applications like maritime heavy-duty engines, Liquefied Natural Gas (LNG), bio- and synthetic fuels will be used primarily [2]. Several studies on the performance of such alternatives have been published in

the last decades, proposing different new concepts or reviewing existing ones and showing promising results.

The extended literature review of Lapuerta et al. [3] presents the advantages of using biodiesel as an alternative to standard diesel fuel. The study concludes that biodiesel can offer a great reduction in carbon monoxide (CO), hydrocarbon (HC), soot and particulate matter (PM) with only a small increase in nitrogen oxides (NO<sub>x</sub>) production. The work of Hoekman and Robbins [4] proposes strategies to mitigate this increase in NO<sub>x</sub> emissions, for example delayed ignition time and use of Exhaust gas recirculation (EGR). In [5] Mwangi et al. present a literature review on the emissions and performance of multiple oxygenated fuels, including diesel and biodiesel mixtures with acetone, butanol, ethanol,

\* Corresponding author.

E-mail address: [Evangelos.Geber.3@city.ac.uk](mailto:Evangelos.Geber.3@city.ac.uk) (E. Geber).

<https://doi.org/10.1016/j.fluid.2023.113888>

Received 8 May 2023; Received in revised form 27 June 2023; Accepted 3 July 2023

Available online 12 July 2023

0378-3812/© 2023 The Author(s). Published by Elsevier B.V. This is an open access article under the CC BY license (<http://creativecommons.org/licenses/by/4.0/>).

Nomenclature	
<b>Abbreviations</b>	
PR	Peng-Robinson
PC-SAFT	Perturbed Chain Statistical Associating Fluid Theory
VLE	Vapor-Liquid Equilibrium
CFD	Computational Fluid Dynamics
LNG	Liquified Natural Gas
EGR	Exhaust gas recirculation
HC	Hydrocarbon
DME	Dimethyl ether
RON	Research octane number
ULSD	Ultra Low Sulphur Diesel
HoV	Heat of vaporization
SRK	Soave-Redlich-Kwong
GC	Group Contribution
HPHT	high-pressure, high-temperature
EoS	Equation of State
QSPR	Quantitative Structure Property Relationship
CO	Carbon Monoxide
OME	Oxymethylene dimethyl ethers
PM	Particulate Matter
MON	Motor octane number
TDP	Tangent Plane Distance
LHV	Lower heating value
<b>Symbols</b>	
$\tilde{a}$	dimensionless Helmholtz free energy
$\beta$	vapor volume fraction
$I_1, I_2$	integrals, functions of density
$\bar{m}$	number of segments
$k^{AB}$	association volume
$\eta$	reduced density
$V$	volume [ $m^3$ ]
$P$	pressure [ $Pa$ ]
$\rho$	density [ $kgm^{-3}$ ]
$c_L$	regression coefficients
$M_w$	molar weight [ $g mol^{-1}$ ]
$f_i$	fugacity
$T$	temperature [ $K$ ]
$\nabla^2 f_k$	Hessian
$x$	liquid phase composition
$N_d$	number of descriptors
C1	abbreviation for the compressibility factor
$m$	number of segments per chain
$\sigma$	segment diameter
$\varepsilon/k$	depth of pair potential
$g_{ii}^{hs}$	radial distribution function
$\varepsilon^{AB}/k$	association energy
$n$	number of groups
$p_k$	direction of Newton method
$z$	composition
$R$	Gas constant [ $J K^{-1} mol^{-1}$ ]
$k_{ij}$	binary interaction parameter
$N_A$	Avogadro number [ $mol^{-1}$ ]
$X^A$	number of molecules not bonded on site A
$\Delta^{A_i B_j}$	the association strength
$\nabla f_k$	gradient
$y$	vapor phase composition
$D_L(\bar{p}_i, \bar{p}_j)$	descriptors QSPR
$m^2 \varepsilon \sigma_d^3$	abbreviation from the PC-SAFT equations
<b>Subscripts</b>	
res	residual
disp	dispersion
assoc	association
id	ideal
ini	initial
hc	hard chain
GC	group contribution
k	iteration number
j	component number j
i	component number i
<b>Superscript</b>	
ref	reference value
l	liquid
*	feed conditions
sat	saturation value
v	vapor
'	trial phase

isopropanol and water. Several studies have pointed out the positive effects of using fuel mixtures like diesel and ethanol or other short chain alcohols. These benefits are mainly the reduction of CO and soot emissions [2,6,7]. Similar improvements can also be achieved in gasoline engines by adding alcohols to gasoline leading to a reduction of CO and HC emissions [8–10]. In [2] Verger et al. also mention Dimethyl ether (DME) and OME as promising alternatives to traditional diesel fuel, however outlining the need for further research on the fuel properties of these oxygenated fuels. A detailed understanding of the relations between the fuel properties, density and internal energy can be a key factor in reaching future environmental goals. The entire fuel injection process can be affected by thermodynamic and transport properties, leading to differences in the fuel/air mixing, in-nozzle cavitation, engine performance and emission levels [3,4,11,12]. The impact of such phenomena has been studied by the authors' group in previous publications [13–16] under the extreme conditions of modern diesel engine injectors, while the work reported in [17–22] deals with measurements and modeling of relevant fuel properties at elevated pressures and temperatures; the vaporization of fuel mixtures has been also investigated [16,23,24].

Because typical commercial fuels are composed of hundreds of hydrocarbons, attempts have been made to create surrogate mixtures to

replicate the real fuel properties. The work of Mueller et al. [25,26] is a good example of such a method, using different parameters like molecular structure, molecular weight, ignition quality, boiling point, melting point, density and viscosity to create a surrogate mixture that replicates the properties of an ultra-low-sulfur diesel reference fuel. In both studies, the fuel surrogates are mixtures of a few components, ranging between four and nine. In [25], the proposed diesel surrogates are split into high and low compositional-accuracy surrogates, based on the number of components and the level of correlation with the target properties that they exhibit. These types of surrogates, both for diesel and gasoline, have been used in computational [16,27] as well as experimental studies [28], allowing a straightforward calculation of fuel properties and reproducibility of the study. Among the various methods available for calculating fuel properties over the wide range of pressure-temperature variation, the PC-SAFT is part of the larger Statistical Associating Fluid Theory (SAFT) EoS family and has been proven to be capable of calculating thermodynamic properties of pure substances and mixtures [29–33]. For the calculation of transport properties, an entropy scaling method using the residual entropy calculated by the PC-SAFT EoS has been proposed [34–36] and has been proven to be a generic as well as accurate method for pure-fuel components. The

PC-SAFT can be easily applied to different fuel components, as it requires only three input parameters ( $m, \sigma, \epsilon/k$ ) per component and a binary interaction coefficient ( $k_{ij}$ ) for each pair. Values for these parameters are available in the literature [29-31,33]. However, if parameter values are not available, the use of a GC method like the one presented by Sauer et al. [37] or by Tihic et al. [38] can be sufficient for estimating ( $m, \sigma, \epsilon/k$ ), while for  $k_{ij}$  the method of Gross and Stavrou [39] can be applied, although the level of precision in complex cases is not clear. Finally, for associating fuel components, two additional inputs are needed for each component, which again can be found in the literature [40] or can be estimated in a similar way [37]. Overall, the PC-SAFT combines precision with a wide range of applicability, making this a very generic EoS. Previous work from the authors' group [16,41-44] has already demonstrated the predictive capability of the PC-SAFT EoS [33], by validating its results against a large variety of multi-component fuels, but also by implementing it into computational fluid dynamics solvers, predicting the in-nozzle flow and subsequent spray development over a wide range of injection and ambient conditions. Properties of multi-component diesel fuel surrogates have been estimated with sufficient precision [45] even under HPHT conditions and by exclusively using GC method estimations for the input parameters. According to the same publication, the PC-SAFT EoS has superior performance compared to the widely used Peng-Robinson (PR) EoS, when calculating liquid density of hydrocarbons. The weakness of cubic EoS like the PR [46] and the Soave-Redlich-Kwong (SRK) [47], related to calculations at HPHT conditions, are also highlighted in [32,48-50]. A series of previous publications by the authors' group [16,27,43,48,51] show that the PC-SAFT can offer sufficient precision when used as thermodynamic closure in a CFD model. The use of the PC-SAFT EoS does come with a substantial computational cost, especially when the EoS is directly implemented in the CFD solver, like in the work of Rodriguez et al. [24]. Alternatively, a tabulated approach can be used to mitigate the increase in computational time by calculating all thermodynamic properties and storing them inside a table in advance. This has been demonstrated in the work of Koukouvinis et al. [48] and Justino et al. [27] with pressure-temperature-composition (P-T-x) tables, as well as in the work of Vidal et al. [16] and Kolovos et al. [51] using two-dimensional density-internal energy ( $\rho$ - $e$ ) tables.

However, in these publications mainly a single component fuel is used, while for the cases of multi-component fuels very limited experimental data for validation are available. The main goal of the present work is to demonstrate the predictive capabilities of the PC-SAFT based thermodynamic model, by extending the limited validation performed in previous studies. A large data set for gasoline and diesel surrogates mixed with short chain alcohols, as well as other oxygenated fuels like OME and a sustainable aviation fuel surrogate is presented for the first time for aviation fuels and used for validation of the computational results. For the gasoline-alcohol mixtures, there are prior computational results using the PC-SAFT but with a pseudo-component methodology, not a fuel surrogate. For OME past results using the PR EoS are available, while for the diesel surrogates there is past work from the authors, but no prior work for mixtures with alcohols, for which there are no prior computational results. The model reported here accounts for the association bonds through the extended PC-SAFT, that includes the association term [40], which allows for the thermodynamic modeling of multicomponent fuel surrogates containing alcohols and other associating components.

## 2. Methods

### 2.1. PC-SAFT formulation

The PC-SAFT is a theoretically derived model, based on perturbation theory. This theory divides the intermolecular potential energy of the fluid into repulsive interactions and attractive interactions. In the PC-

SAFT a reference fluid is defined to calculate the repulsive contribution. The reference fluid is composed of spherical segments comprising a hard sphere fluid that then forms molecular chains to create the hard-chain fluid. The attractive interactions, perturbations to the reference system, are accounted for with the dispersion term [33]. In addition to these two basic terms, the association term can be also included [40] to account for the intermolecular bonds forming between hard-sphere segments with association sites (proton donor and acceptor). The hydrogen bonds formed by the -OH group of alcohols are an example of self-association [52] that will be modeled in this work.

The PC-SAFT EoS is based on Helmholtz free energy, which in turn is derived as the sum of the hard chain, dispersion and association contributions shown in Eq. (2.1):

$$\tilde{a}_{res} = \tilde{a}_{hc} + \tilde{a}_{disp} + \tilde{a}_{assoc} \quad (2.1)$$

The hard-chain term,  $\tilde{a}_{hc}$ , for a mixture of  $nc$  components, is given by Eq. (2.2):

$$\tilde{a}_{hc} = \bar{m} \tilde{a}_{hs} - \sum_i^{nc} x_i (m_i - 1) \ln g_{ii}^{hs}(\sigma_{dii}) \quad (2.2)$$

where  $\bar{m}$  is the number of segments for a multicomponent mixture,  $x_i$  is the mole fraction of every component  $i$  in the fluid,  $\tilde{a}_{hs}$  is the hard sphere contribution,  $g_{ii}^{hs}$  is the radial distribution function of the hard-sphere fluid and  $m_i$  is the number of segments per chain of every component. The dispersion term is defined by Eq. (2.3):

$$\tilde{a}_{disp} = -2\pi\rho_m I_1(\eta, \bar{m}) m^2 \epsilon \sigma_d^3 - \pi\rho_m \bar{m} C_1 I_2(\eta, \bar{m}) m^2 \epsilon^2 \sigma_d^3 \quad (2.3)$$

According to [52-54] the association contribution to the Helmholtz free energy is an average that is linear with respect to mole fractions and can be derived by Eq. (2.4).

$$\frac{\tilde{a}_{assoc}}{RT} = \sum_i X_i \left[ \sum_{A_i} \left[ \ln X^{A_i} - \frac{X^{A_i}}{2} \right] + \frac{M_i}{2} \right] \quad (2.4)$$

Where  $M_i$  is the number of association sites on each molecule of component  $i$  and  $X^{A_i}$ , the mole fraction of molecules not bonded at site  $A$  for component  $i$ , is given by:

$$X^{A_i} = \left[ 1 + \sum_j \sum_{B_j} \rho_j X^{B_j} \Delta^{A_i B_j} \right]^{-1} \quad (2.5)$$

Where  $\sum_{B_j}$  represents summation over all sites on the molecules of component  $j$ :  $A_j, B_j, C_j$  etc. Also  $\rho_j = X_j \rho_{mixture}$  is the molar density and  $\Delta^{A_i B_j}$  the association strength. Lastly, the mixture parameters  $\sigma_{ij}$  and  $\epsilon_{ij}$  which are defined for every pair of unlike segments are modelled using a Berthelot-Lorentz combining rule.

$$\sigma_{ij} = \frac{1}{2} (\sigma_i + \sigma_j) \quad (2.6)$$

$$\epsilon_{ij} = \sqrt{\epsilon_i \epsilon_j} (1 - k_{ij}) \quad (2.7)$$

where  $k_{ij}$  is the binary interaction parameter. The mixture parameters are used for the computation of  $m^2 \epsilon^2 \sigma_d^3$  in Eq. (2.3). For more information on the derivation of the PC-SAFT EoS equations the reader is directed to the original publication of the model [33,40].

### 2.2. PC-SAFT parameter estimation

The main input parameters needed for the PC-SAFT calculations are the number of segments per chain ( $m$ ), the segment diameter ( $\sigma$ ) and the depth of pair potential divided by the Boltzmann constant ( $\epsilon/k$ ) and they must be defined for each component individually. Values that have been

adjusted using experimental density and vapor pressure data can be found in the literature [30,33,40]. However, the goal of this work is to present a generic and predictive methodology for fuel-property calculation, thus a GC method is applied for the estimation of the input parameters. The GC method of Tihic et al. [38] is implemented in this work, with overall good results based on past experience. In this approach, the chemical structure of the molecule is divided into simple, first-order groups and more complex, second-order groups. The PC-SAFT parameters  $m$ ,  $\sigma$  and  $\varepsilon/k$  are computed as a function of all the individual group contributions  $m_i$ ,  $\sigma_i$  and  $\varepsilon/k_i$  according to the following set of equations:

$$\mathbf{m} = \sum_i^n \text{groups} (n_i m_i)_{FOG} + \sum_i^n \text{groups} (n_i m_i)_{SOG} \quad (2.8)$$

$$\mathbf{m}\sigma^3 = \sum_i^n \text{groups} (n_i m_i \sigma_i^3)_{FOG} + \sum_i^n \text{groups} (n_i m_i \sigma_i^3)_{SOG} \quad (2.9)$$

$$m \varepsilon / k = \sum_i^n \text{groups} (n_i m_i \varepsilon / k_i)_{FOG} + \sum_i^n \text{groups} (n_i m_i \varepsilon / k_i)_{SOG} \quad (2.10)$$

The computation of the individual group contributions relies on fitting of vapor pressure and liquid density data at a reduced temperature range of  $0.5 \leq T_r \leq 0.9$ .

The work of Burgess et al. [55], which is an extension of the previously mentioned method, is also used in cases where a weak performance of the thermodynamic model is observed. While the above equations are also valid in this situation, the values of  $m_i$ ,  $m_i \sigma_i^3$  and  $m_i \varepsilon / k_i$  for each first order group and second order group are different. The method of Burgess et al. [55] aims to improve the performance under high- and low-pressure conditions, by creating two different sets of GC parameters, one derived based on experimental data at low pressure (lower than 7 MPa) and one at high pressure conditions (7 MPa up to 276 MPa). In this work the GC parameters corresponding to low pressure conditions are used since the experimental data for the C-1 surrogate, for which this approach is later used, are all well below 7 MPa.

For OME<sub>n</sub> fuel family a model developed by Schappals et al. [56] is also investigated as a possible solution. In this approach, the number of segments  $m$  in OME<sub>n</sub> is assumed to be linearly dependent on the OME chain length  $n$  and the parameters  $\sigma$  and  $\varepsilon/k$  are considered constant. This is a rather simple approach, which has been developed through fitting of experimental vapor pressure and liquid density data, at a temperature range of 300–500 K and pressure of 1 bar and below. Thus, it serves as a good reference for comparison with the more generic GC method. All the input parameters of the individual components for the PC-SAFT formulations can be found in the Appendix Tables 4–6.

For associating components, the bonding type must be defined. For alkanols, which are the main type of substances we want to study, the 3B and 2B bonding model is proposed by Huang et al. [53]. Since the use of the complex 3B could not be sufficiently justified, the simpler 2B was used in this work. Also, the study of Gross et al. [40] uses the 2B model with great success to describe substances like ethanol, methanol, pentanol etc. Thus, the 2B bonding approach was selected as the most suitable option for this work. Two additional pure component parameters, the effective association volume ( $k^{AB}$ ) and the association energy ( $\varepsilon^{AB}/k$ ) are used for associating components. Those can also be computed using the GC method proposed by Tihic et al. [38]. Finally, for the estimation of the binary interaction parameter ( $k_{ij}$ ) the method of Stavrou et al. [39] was used. In the proposed Quantitative Structure Property Relationship (QSPR) method, the  $k_{ij}$  is calculated by the following equation:

$$k_{ij}^{QSPR} = \sum_{L=1}^{N_d} c_L D_L(\bar{p}_i, \bar{p}_j) \quad (2.11)$$

Where  $N_d$  is the number of descriptors,  $D_L(\bar{p}_i, \bar{p}_j)$  are the descriptors and  $c_L$  are corresponding regression coefficients. The descriptors are functions of the PC-SAFT molecular parameters. Since all fuel mixtures have no-polar components and only up to a single associating component, one descriptor needs to be used, which is calculated as below:

$$D^{LJ} = 1 - \left[ \frac{\sigma_i^3 (\varepsilon_i/k)^2}{\sigma_j^3 (\varepsilon_j/k)^2} \right] \quad (2.12)$$

The value of the  $c^{LJ}$  coefficient can be found from tables in the work of Stavrou et al. [39].

### 2.3. VLE calculations

The methodology presented here was developed and published by the authors, as reported by Vidal et al. in [42]. The vapor-liquid equilibrium calculations are performed under constant temperature, specific volume, composition and are based on the unconstrained minimization of the Helmholtz free energy. The choice of temperature, specific volume or density and compositions as independent variables is suitable as in the PC-SAFT all equations are expressed as functions of the same variables. More importantly, the use of density instead of pressure as an independent variable allows for better description of phase change. In the case of a single component or a multi-component mixture with very similar components, phase change occurs at constant pressure or almost constant pressure respectively, requiring a pressure-based code to calculate only a single point in vapor-liquid equilibrium and reducing the entire phase change process to one state.

The algorithm consists of two stages, namely the stability analysis and the flash calculations. First, the mixture is assumed to be in a single-phase state and its stability is investigated through the Tangent Plane Distance (TPD), in a similar way to the work of Michelsen and Mollerup [57]. If the TDP, which can be calculated according to Eq. (2.13), is proven to be always non-negative the mixture can be considered stable. Otherwise, it is unstable and the flash calculations follow to determine the composition of the two-phase mixture. The existence of a non-negative minimum of the TPD is enough to prove that the mixture is stable and thus, this can be seen as a minimization problem.

$$TPD = \frac{P' - P^*}{RT} + \sum_{i=1}^{nc} \rho x_i' (\log f_i' - f_i^*) \quad (2.13)$$

In Eq. (2.13), the primes refer to the trial phase and the asterisk the feed conditions.  $R$  is the universal gas constant,  $f_i$  is the fugacity of the component  $i$ ,  $P$  the pressure,  $\rho$  density and  $nc$  the number of components. For the initialization of the iterative minimization process Raoult's law and Wilson's correlation [58] are combined with the work of Michelsen [59] and of Mikyska and Firoozabadi [60] to obtain the expression for initial composition of liquid ( $y_i$ ) and vapor phase ( $x_i$ ), where  $z_i$  stands for the total initial composition:

$$x_i = \frac{z_i P_{ini}}{P_i^{sat}} = \frac{z_i}{P_i^{sat} \left( \sum_{i=1}^{nc} \frac{z_i}{P_i^{sat}} \right)}, \quad (2.14)$$

$$y_i = \frac{z_i P_i^{sat}}{P_{ini}} = \frac{z_i P_i^{sat}}{\sum_{i=1}^{nc} z_i P_i^{sat}}$$

If a two-phase regime is detected during the stability analysis, the code proceeds with the flash calculations aiming at minimizing the Helmholtz Energy for a given density, temperature and composition. Through the flash calculations the vapor mole fraction  $\beta = \sum_{i=1}^{nc} n_i^v$  is computed and from there the composition (Eq. (2.15)) and density (Eq. (2.16)) of the liquid and vapor phase can be derived, where  $v$  stands for vapor and  $l$  for liquid phase.

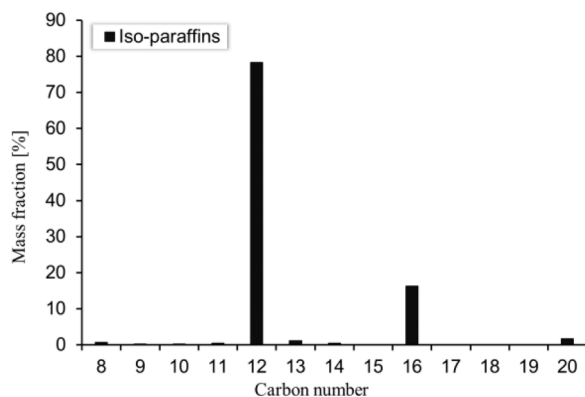


Fig. 1. Composition of alcohol-to-jet C1 sustainable aviation fuel.

Table 1

Main properties of alcohol-to-jet C1 and its surrogate.

	C1 ATJ FUEL	SURROGATE
Formula	$C_{12.5}H_{27.1}$	$C_{12.5}H_{27.1}$
H/C ratio	2.168	2.159
A/F <sub>stoich</sub>	14.902	14.966
MW [g/mol]	178.0	177.5
LHV [MJ/kg]	43.88	44.09
HoV [MJ/kg]	0.35	0.278
Heat capacity (liquid) at 20 °C [kJ/kgK]	1.96	1.96
Surface tension at 22 °C [N/m]	0.0234	0.0222
Flash point [ °C]	49.5	62.7
Freeze point [ °C]	-61.0	-60.3
Derived Cetane #	16.0	16.4
Smoke point [mm]	34.5	34.4

$$x_i = \frac{n_i^v}{\beta}, \quad y_i = \frac{n_i^l}{\beta} \quad (2.15)$$

$$\rho^v = \frac{\beta}{V^v}, \quad \rho^l = \frac{1 - \beta}{V^l} \quad (2.16)$$

In both cases, stability and flash, the optimization problem is solved using Newton's method (c.f. [61]). For the calculation of the step length of the Newton method, an inexact line search is performed to calculate a step length that satisfies the Wolfe conditions [62]. The equation that needs to be solved to calculate the direction ( $p_k$ ) is:

$$\nabla^2 f_k p_k = -\nabla f_k \quad (2.17)$$

Where  $\nabla^2 f_k$  is the Hessian and  $\nabla f_k$  is the gradient of the objective function that is to be minimized. In order for the above system to have a solution, the Hessian must be positive definite. To ensure that the Hessian is a positive definite matrix we use the modified Cholesky factorization algorithm [63].

#### 2.4. Sustainable aviation fuel surrogate formulation

A surrogate fuel for alcohol-to-jet sustainable aviation fuel was developed in this investigation. Alcohol-to-jet, named C1 by the National Jet Fuels Combustion Program NJFCP (POSF number 11,498), is a bio-derived kerosene-like fuel mainly composed by highly branched C12 and C16 isoparaffins and with very low autoignition reactivity compared to standard petroleum-based kerosene. The composition and main properties of C1 are shown in Fig. 1 and Table 1, respectively.

The surrogate fuel for C1 is formulated following a similar approach to that described in [68]. An initial surrogate formulation is defined based on the composition of the fuel and using a palette of components for which detailed chemical kinetic models are available. For C1, the selected components were 2,2,4,6,6 pentamethyl heptane (aka

isododecane) and 2,2,4,4,6,8,8 heptamethyl nonane (aka isocetane). Then, the composition of this initial surrogate is adjusted in an iterative process until the surrogate matches several user-specified property targets of the real fuel. In this investigation, the surrogate targets were the derived cetane number (for autoignition reactivity), the smoke point (for soot propensity), and the density, viscosity and vapor pressure (for spray behavior). Fig. 2 shows the density, kinematic viscosity and vapor pressure of C1 compared to those of the surrogate. The smoke point of the surrogate is estimated by a linear mass-fraction blending rule, the viscosity of the surrogate is estimated by the Kendall-Monroe equation, and the vapor pressure of the surrogate is estimated by the Hoffmann-Flurin equation. The properties of the real fuel were obtained from [64] (measured values).

A new method to predict the derived cetane number of a fuel is introduced in this study and used to estimate the derived cetane number of the surrogate. First, the mixture fraction vs. temperature distribution within a fuel spray is calculated at the conditions of the derived cetane number test (ambient temperature equal to 817 K, pressure equal to  $2.14 \times 10^6$  Pa) using a 1D spray model [65]. Then, the ignition delay that corresponds to each mixture fraction – temperature combination is obtained in a 0D closed homogeneous reactor using a detailed chemical kinetic mechanism from LLNL [66]. Finally, the ignition delay of the most reactive mixture fraction, i.e., the mixture fraction with the shortest ignition delay time, is correlated with the derived cetane number of the fuel using a correlation curve calibrated for more than 50 fuels and binary fuel blends with known derived cetane number (shown in Fig. 3). The estimated derived cetane number of the surrogate, together with other properties, are compared against those of the real C1 fuel in Table 1.

### 3. Results and discussion

A series of computational results are presented for liquid and saturation density, vapor pressure and distillation curves of wide range of fuels, such as gasoline, diesel and aviation fuel surrogates, gasoline and alcohol blends, as well as a highly-oxygenated fuels (OME<sub>3-4</sub>). All the simulated gasoline fuels and mixtures with alcohols are listed in Table 2, including their individual components and molar composition. Table 3 presents analog information, but for the diesel and aviation fuel surrogates, together with diesel/alcohol blends.

The results are compared with experimental measurements and data generated by other computational models for validation. In this way, the reliability of the thermodynamic model can be assessed. It should be noted that, for simplicity, the absolute difference expressed as a percentage is referred to as the error or deviation in this section.

As mentioned previously in Section 2.2, different methods to determine the input parameters of the model have been used, in cases where a weak performance of the thermodynamic model was seen. It should be noted that this is more of an investigation for the impact these models can have not an attempt to optimize the results based on a specific criterion. The authors have designed the model with the intention to use it coupled with a CFD solver in future publications, thus the acceptable level of accuracy would be defined by the outcome of the complete CFD simulations. In this paper, cases with a comparatively bigger room for improvement were selected for the investigation of different parameter estimation methods.

#### 3.1. Distillation curves

All the distillation curves presented are calculated according to the ASTM D86 standard test method [67]. Thus, a simulation of the experimental procedure is performed as follows: the fuel temperature is set below the initial boiling point and the pressure is set equal to atmospheric. Then, an incremental increase of fuel temperature is applied until a two-phase regime is reached, marking the start of the

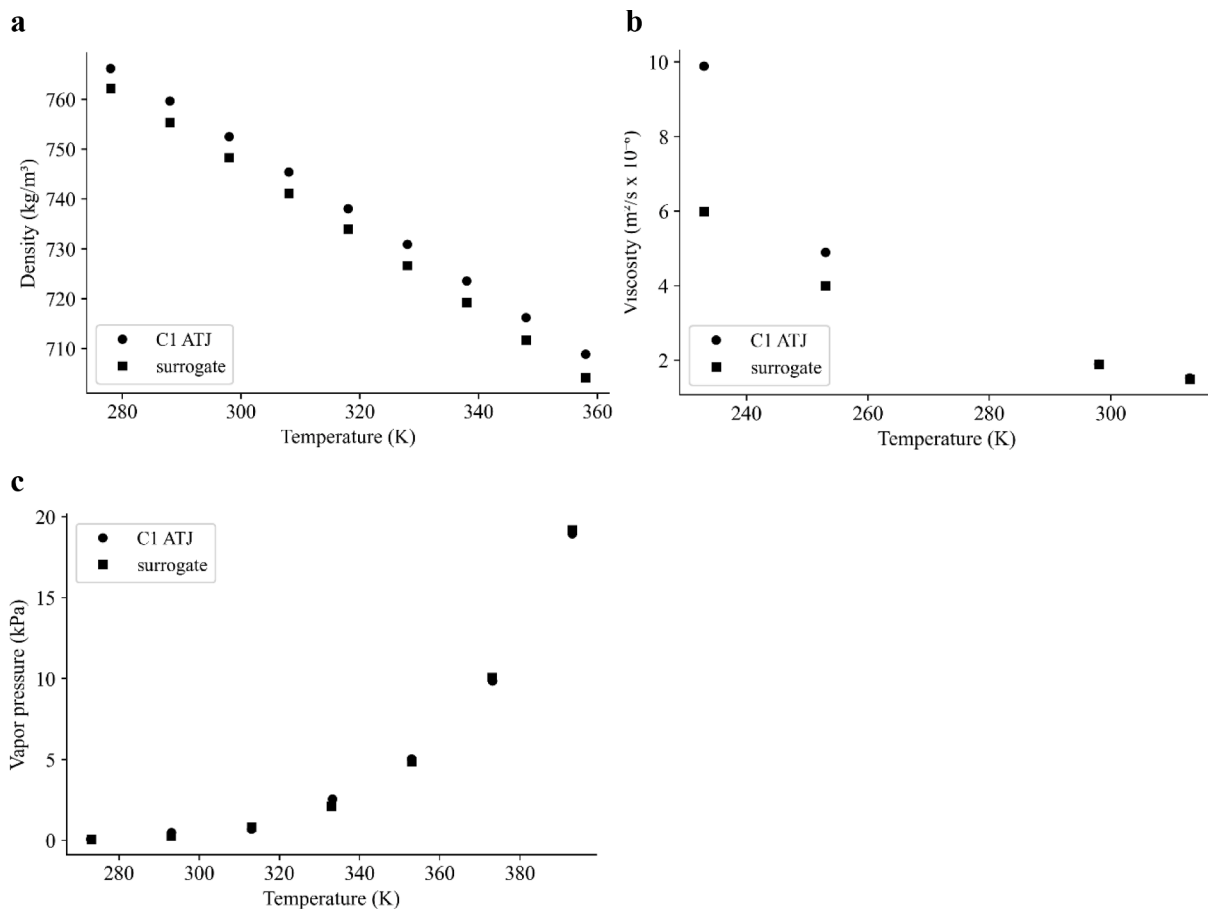


Fig. 2. (a) Density, (b) kinematic viscosity and (c) vapor pressure of C1 fuel (measured values from [64] and the surrogate).

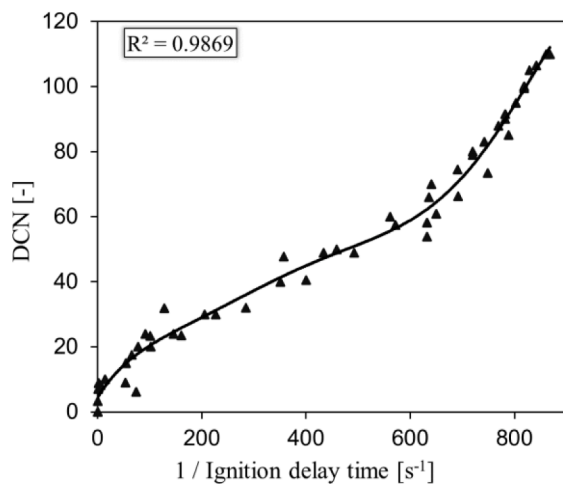


Fig. 3. Correlation between derived cetane number and ignition delay of the most reactive mixture fraction for more than 50 fuels and binary fuel blends.

evaporation. In the experimental procedure, the vapor is captured, cooled down to 20 °C and its volume is measured. In the simulation, the computed composition of the vapor phase is used as input for a new calculation at 20 °C to compute the molar volume. The composition of the remaining liquid phase is used for the next step, where the temperature is increased again, and new vapor and liquid phase compositions are computed. This incremental temperature increase is performed until complete evaporation. In every step the molar vapor fraction and the molar volume of condensed vapor are calculated, which together

with the total liquid volume are used to calculate the distilled volume fraction.

In this section the results for blends of gasoline and short-chain alcohols are presented. The alcohols used are methanol and ethanol, with a volumetric concentration ranging from 10% to 50%. For the modeling of gasoline, different fuel surrogates are used depending on the available experimental data. All calculations are performed using the GC-PC-SAFT, with the pure component parameters being estimated according to the correlations published by Tihic et al. [38]. For the experimental measurements presented in Fig. 5 and Fig. 6, a reference gasoline (Halterman EEE) was used. The exact composition of this gasoline is too complicated to model and thus the E00 gasoline surrogate is used instead for the PC-SAFT predictions. This 3-component surrogate has been shown to properly replicate the properties of Halterman EEE gasoline [28], with some inevitable weaknesses due to the simplified composition.

In Fig. 4 the distillation curves of pure E00 and EEE gasoline are presented, illustrating the inherent differences between the surrogate and the actual fuel. These should be noted as they will appear as well in the following graphs; however, they are limitations of the surrogate and not of the computational model. Fig. 4 shows that the results of the thermodynamic code match the experimental measurements for the E00 surrogate.

In Fig. 5, a comparison of PC-SAFT predictions against measurements for the distillation curves of E10 (ethanol mixed with gasoline at 10% v/v concentration) and M10 (methanol mixed with gasoline at 10% v/v concentration) is presented. It can be concluded that overall, there is reasonable agreement between experimental data and the calculations of the thermodynamic code. Significant differences are only present at the start and the end of the vaporization process and can be attributed to

**Table 2**  
Molar composition of all simulated gasoline fuel surrogates and mixtures.

Compound	E00	E10	M10	PACE1	PACE8	PACE20
n-pentane	46.1%	35.9%	32.7%			
isooctane	41.3%	32.2%	29.3%	15.5%	18%	17.6%
n-undecane	12.6%	9.8%	8.9%			
ethanol		22.1%		19.3%	19.4%	18.9%
methanol			29.1%			
isopentane				7.8%	10.7%	13.9%
cyclopentane				13.5%	10.8%	13%
hexene				6.3%	5.1%	5%
toluene						10.1%
heptane				15.3%	13.9%	9.1%
1,2,4-trimethylbenzene				22.3%	22.1%	9.9%
tetralin						2.5%

**Table 3**  
Molar composition of simulated diesel and aviation fuel surrogates and mixtures.

Compound	V0b	V0b+ methanol	V0b+ ethanol	V0b+ propanol	V0b+ butanol	V0b+ pentanol	C-1
octadecane	23.5%	9.8%	11.9%	13.4%	15.5%	15.4%	
heptamethyl nonane	27%	11.2%	13.7%	15.4%	16.7%	17.7%	16.4%
1-methylnaphthalene	16.1%	6.7%	8.2%	9.1%	9.9%	10.6%	
tetralin	20.9%	8.7%	10.6%	11.9%	12.9	13.7%	
1,2,4-trimethylbenzene	12.5%	5.2%	6.4%	7.1%	7.7%	8.2%	
methanol		58.4%					
ethanol			49.2%				
propanol				43.1%			
butanol					38.3%		
pentanol						34.4%	
pentamethyl heptane							83.6%

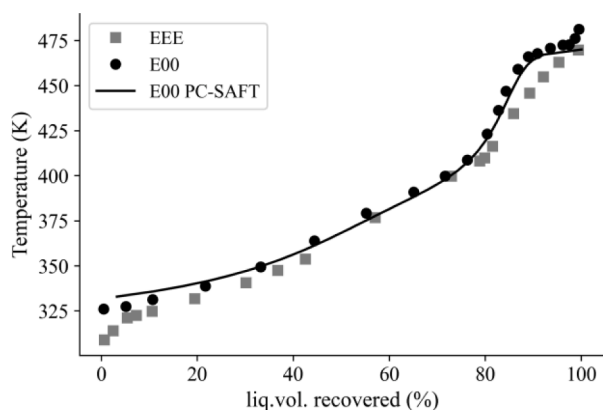


**Fig. 4.** Comparison of PC-SAFT predictions against experimental measurement for the distillation curve of E00 gasoline surrogate. Measurements corresponding to EEE reference gasoline are also presented [68].

the use of a surrogate instead of the actual gasoline fuel in the PC-SAFT model. This is evident from Fig. 4, where the distillation curve of E00 exhibits the same differences when compared to EEE gasoline, an overestimation of the initial boiling point at 325 K and an overall notable deviation above 425 K. Similar conclusions can be drawn about the E20 and E50 (ethanol concentration at 20% and 50% v/v respectively) fuel mixtures, from Fig. 6. The inflection point has moved to a higher distilled volume compared to the E10 sample due to the higher content of ethanol, but the thermodynamic code is still able to capture this behavior.

This deviation from the experimental data at the start and end of the vaporization process can be explained by looking into the composition of the gasoline fuel and the simplified surrogate. An authentic gasoline fuel is composed of a multitude of elements, each differing substantially in their boiling points. The highest and lowest boiling points among

these components will dictate the initial and final boiling points, respectively. However, these extremes considerably diverge from the boiling points of elements found within surrogate fuels.

The discrepancy discerned around the inflection point could be attributed to a suboptimal estimation of the binary interaction parameter  $k_{ij}$  or the use of a surrogate mixture. The  $k_{ij}$  value must be estimated for each pair of components, in this case corresponding to six different values. A small under- or over- estimation can affect the result of the calculations. Another explanation would be the use of a surrogate mixture which doesn't consist of all the components of the original fuel. This could mean a slightly different interaction with ethanol/methanol and a small discrepancy in the predicted evaporation of the alcohol part.

In the second set of experimental measurements the fuel surrogates PACE-1, PACE-8 and PACE-20 [67] are presented. All of them aim at replicating the properties of RD5–87, a research-grade gasoline containing 10% vol/vol ethanol, representative of the majority of commercial gasoline in the US [70]. PACE-1 and PACE-8 consist of 7 individual components while PACE-20 is made up of 9 h, with the composition being tailored so that the surrogate fuels match research/motor octane numbers (RON/MON) and other combustion targets of RD5–87 [70]. Since the composition of these fuel surrogates is known, there is no need to further simplify the modeling as was done in the previous case.

In Fig. 7 we see that for all cases there is very good agreement between the experimental measurements and the results of the thermodynamic model. A notable difference appears only at the start of vaporization, where the computational model tends to overpredict the initial boiling point by up to 6%. This deviation is deemed acceptable, especially if we consider that a very similar level of accuracy is achieved by the Lawrence Livermore National Laboratory (LLNL) simulations [71].

In this section the results for blends of diesel and five short-chain alcohols are presented. The alcohols used are methanol, ethanol, propanol, butanol and pentanol, with a volumetric concentration of 20%. For the modeling of the diesel, a fuel surrogate is needed because its exact

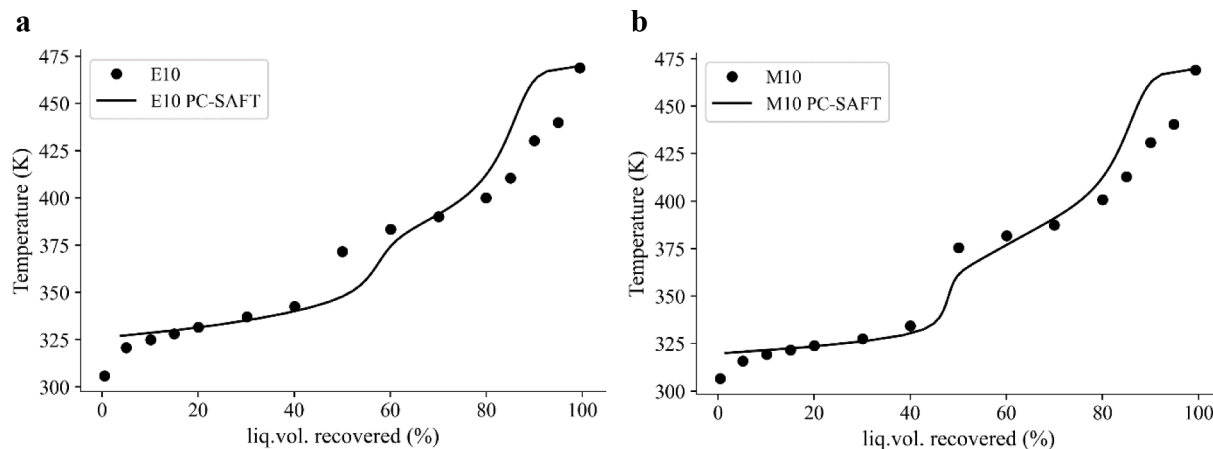


Fig. 5. Comparison of PC-SAFT predictions against experimental measurement for the distillation curve of E10 (a) and M10 (b) [69].

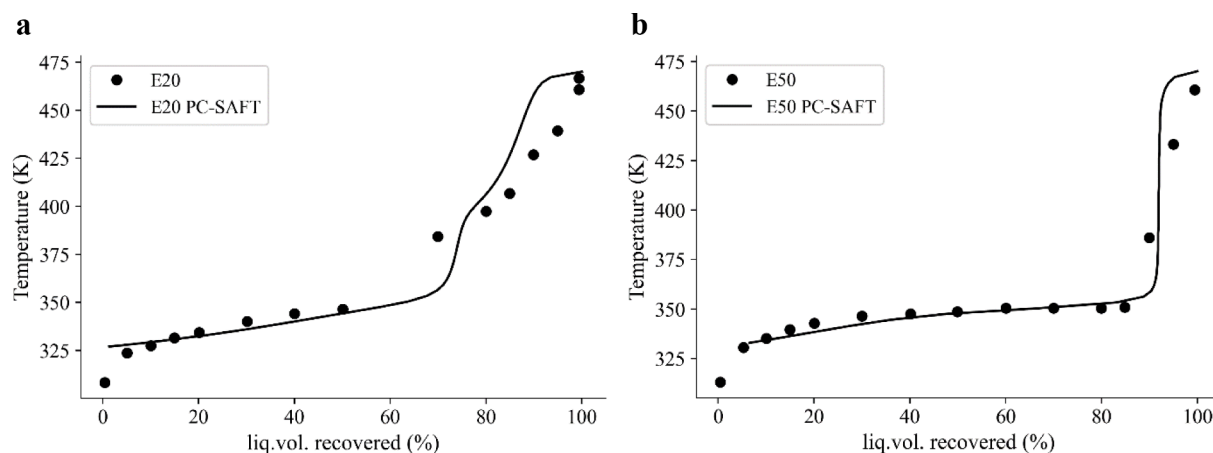


Fig. 6. Comparison of PC-SAFT predictions against experimental measurement for the distillation curve of E20 (a) and E50 (b) [69].

composition cannot be estimated with good accuracy. Since an Ultra Low Sulfur Diesel (ULSD) was used during the experimental procedure [72], the V0b diesel surrogate was used in the computational model. This specific fuel surrogate was developed by Mueller et al. [26] and in a previous study by Vidal et al. [45] it was found to have properties representative of ULSD. Also, like in the previous section, the GC theory model of Tihic et al. [38] is used. A comparison between the distillation curve of the ULSD published by [72] and V0b is done, in order to identify what discrepancies can be attributed to the simplification of using a surrogate. Looking at Fig. 8 it is evident that the distillation curve of V0b is not following closely the distillation curve of ULSD. While the difference in temperature remains at around 3% for a recovered volume under 70%, it can reach up to 10%, or 65 K, at 98% recovered volume. Rather than perfectly replicating the behavior of the specific diesel, the goal here is to achieve a similar behavior to the original diesel and study the influence of mixing with alcohols.

When comparing the computational results to the experimental measurements of V0b, a difference of 7% or 38 K is obtained for the initial boiling temperature. This discrepancy slowly decreases at a higher distilled volume, with the final boiling temperature exhibiting only a 2% or 11 K difference.

The impact of adding different alcohols into the diesel fuel can be seen in Fig. 9. The change in the initial boiling point as well as the inflection point, caused by the alcohol's evaporation, is captured by the computational model in all five cases. However, with an increasing number of carbon atoms in the alcohol, a small discrepancy gradually appears around 20% recovered volume. This error at the inflection point

reaches a maximum value of 9%, or 40 K, when using pentanol as the mixture component. This can be deemed acceptable, especially if we consider a similar uncertainty from the computational model published by Hernández et al. [72]. The use of a surrogate instead of the actual diesel fuel is responsible for the differences at higher distilled volumes, above 50%. This can be understood by going back to Fig. 8, where it is evident that, for a specific distilled volume, the measured temperature for the ULSD is higher than the computed temperature of the V0b surrogate at the same distilled volume.

A comparison between experimental measurements and computational results for the distillation curve of a two-component surrogate of the aviation fuel C-1 is presented below. C-1 is an alcohol-to-jet (ATJ) fuel containing highly branched dodecane and hexadecane type components, crafted by the National Jet Fuels Combustion Program NJFCP [73]. The C-1 ATJ fuel was designed to represent alternative jet fuels in experimental procedures, with the goal of developing non-fossil-based jet fuel alternatives [74]. These non-conventional fuels can be a potential solution to limiting the impact of anthropogenic carbon from the aviation transportation sector [74].

The composition of the surrogate, representative of C-1 ATJ, is listed in Table 3 together with the other fuels presented in this work. While in the previous cases of gasoline alcohol mixtures the GC parameterization method of Tihic et al. [38] performed very well, here we see a significant over prediction of the temperature at all volume fractions, refer to Fig. 10. The error in temperature reaches a maximum value of 12% at a recovered volume fraction of 50% and the deviation is 10% on average. Thus, the GC methodology developed by Burgess et al. [55] is also

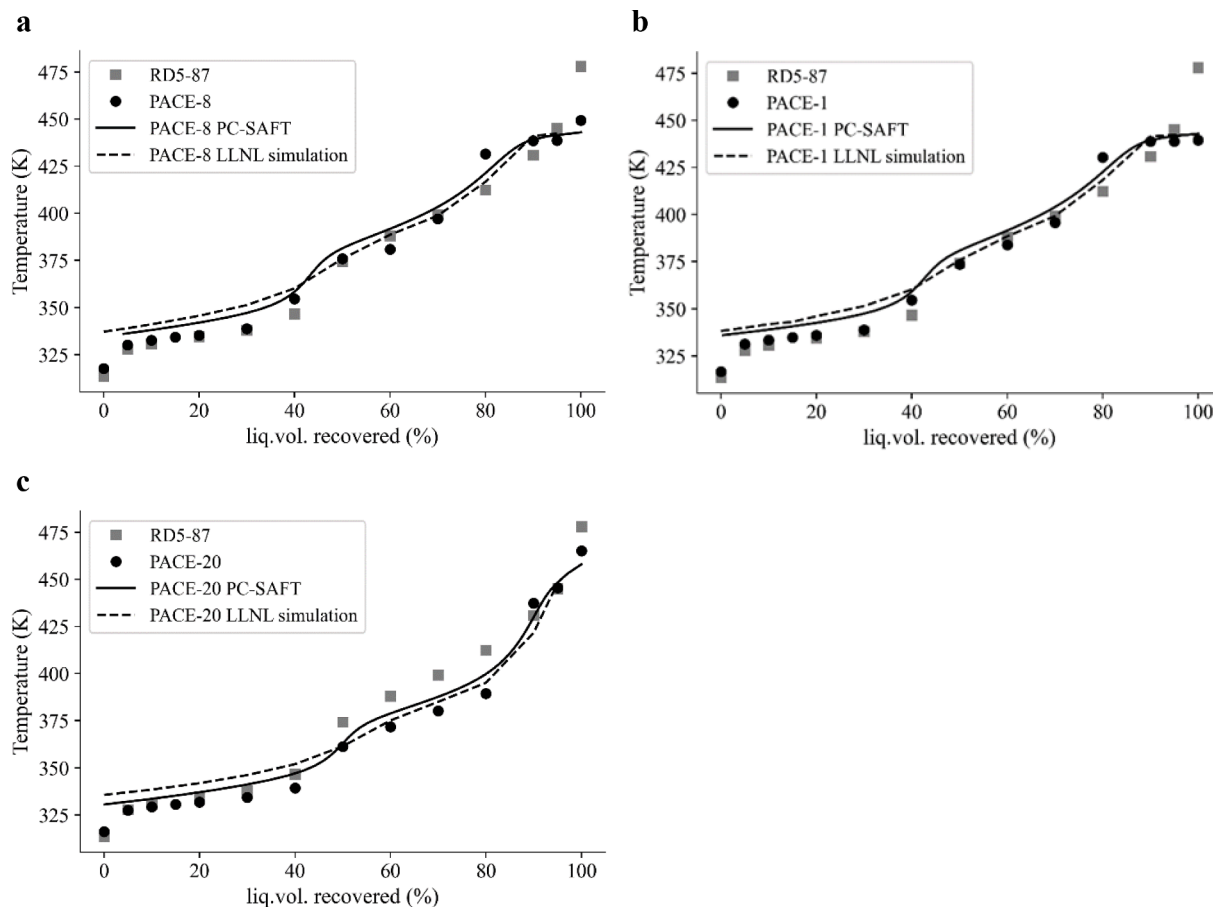


**Fig. 7.** Comparison of PC-SAFT predictions against experimental measurement for the distillation curve of PACE-1 (a) and PACE-8 (b) and PACE-20 (c) [70]. The measurements corresponding to RD5–87 reference gasoline/ethanol mixture are also presented.

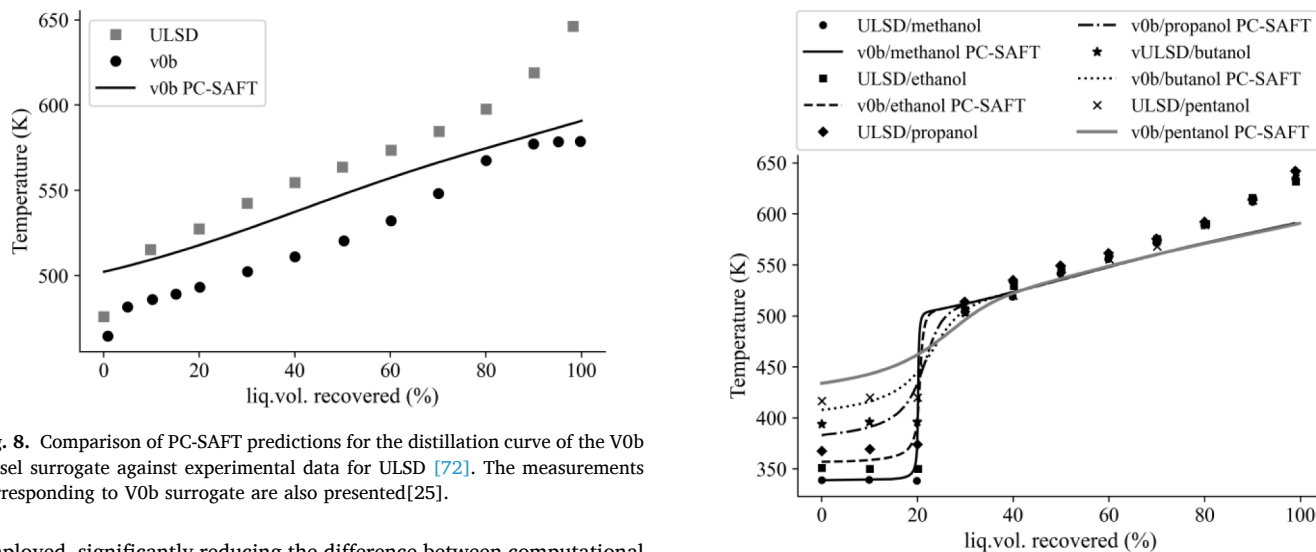


**Fig. 8.** Comparison of PC-SAFT predictions for the distillation curve of the V0b diesel surrogate against experimental data for ULSD [72]. The measurements corresponding to V0b surrogate are also presented [25].

employed, significantly reducing the difference between computational and experimental results, achieving a maximum and average error of 4% and 1%, respectively.

### 3.2. Density

In this section density data as a function of temperature for OME<sub>3</sub>, OME<sub>4</sub> and the surrogate of C-1 are presented and compared to the PC-SAFT results. Different methods for the estimation of the pure

**Fig. 9.** Comparison of PC-SAFT predictions for the distillation curve of the V0b diesel surrogate mixed with alcohols against experimental data ULSD/alcohol blends [72]. The short chain alcohols used are methanol, ethanol, propanol, butanol and pentanol.

component parameters are employed, to investigate which options yield the most reliable results. Similar to the case of the distillation curve, the use of the GC method of Tihic et al. [38] for the surrogate of C-1 leads to

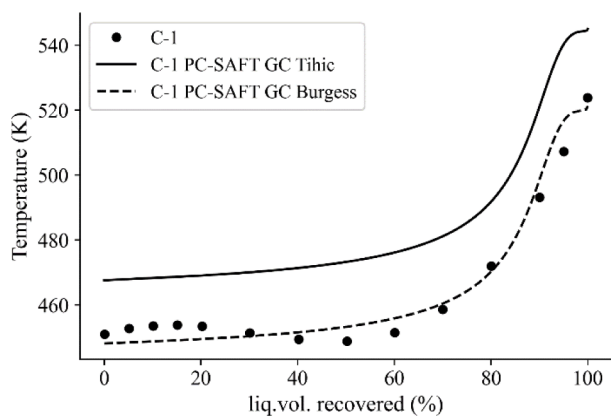


**Fig. 10.** Comparison of PC-SAFT predictions for the distillation curve of the surrogate of C-1 against experimental data. The GC method of Tihic et al. [38] and the of Burgess et al. [55] were used.

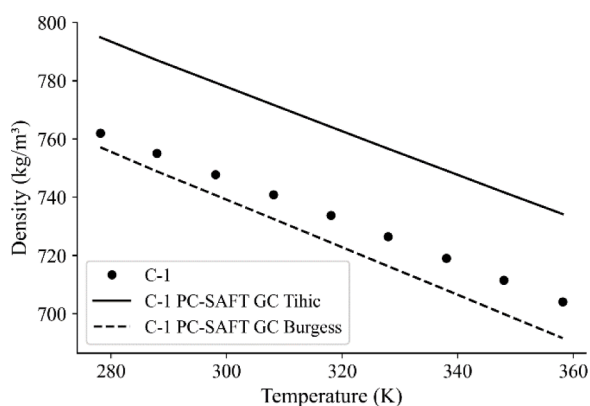


**Fig. 11.** Comparison of PC-SAFT predictions for the density, as a function of temperature at atmospheric pressure, of the surrogate of C-1 against experimental data. The GC methods of Tihic et al. [38] and the of Burgess et al. [55] were used.

an overestimation of the liquid density and has an overall maximum error of 4.3%, with the average error being 4.2%, see Fig. 11. In contrast, using the method of Burgess et al. [55] a smaller maximum and average error of 1.8% and 1.2% is achieved.

For OME<sub>3</sub> and OME<sub>4</sub> the saturation density is calculated using the GC method of Tihic et al. [38], as well as the parametrization method

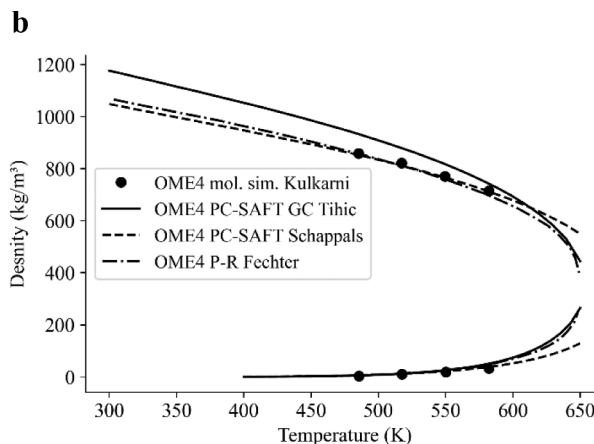
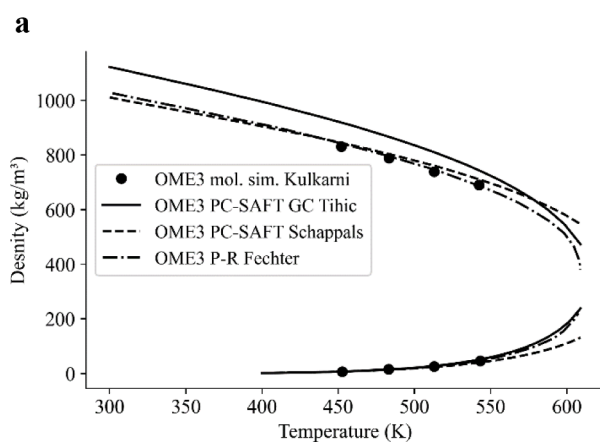


**Fig. 12.** Comparison of PC-SAFT predictions for the OME<sub>3</sub> (a) and OME<sub>4</sub> (b) saturation density against computational results of Fechter et al. [75] (PR EoS) and the molecular dynamics simulations of Kulkarni et al. [76]. The GC method of Tihic et al. [38] and the parametrization of Schappals et al. [56] were used.

proposed by Schappals et al. [56], refer to Fig. 12a. As expected, the second method leads to a better estimation of the saturation density, as it is designed specifically for the OME chemical family. Nevertheless, even with the method of Tihic et al. [38] the deviation when compared to the PR EoS calculations of Fechter et al. [75] is about 10% at low temperatures (300 K) but decreases substantially above 500 K for OME<sub>3</sub>, with the density predicted by the PC-SAFT model remaining consistently higher.

A similar trend is observed in the results for OME<sub>4</sub> in Fig. 12b, with an error of 10% at low temperatures (300 K) for the method of Tihic et al. [38] and a significant decrease of this error above 550 K, while the method of Schappals et al. [56] leads to an approximately 10 times smaller deviation. However, it should be noted that around the critical point the method of Schappals et al. [56] is no longer superior, as it starts to produce results with a larger discrepancy compared to the curve of Fechter et al. [75] produced using the PR EoS. The computational results of Fechter et al. [75] are in good agreement with the molecular dynamics simulations of Kulkarni et al. [76], but cover a much larger temperature range. Thus, they are considered a good benchmark for comparison and evaluation of the computational results obtained in this work.

### 3.3. Vapor pressure

Experimental data for vapor pressure of the C-1 surrogate, OME<sub>3</sub> and

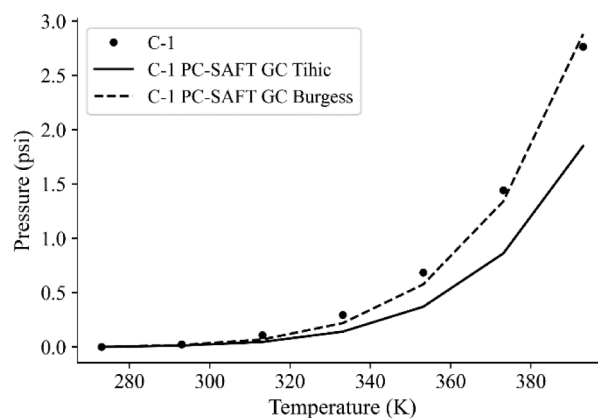


**Fig. 13.** Comparison of PC-SAFT predictions for the vapor pressure, as a function of temperature, of the surrogate of C-1 against experimental measurements. The GC methods of Tihic et al. [38] and of Burgess et al. [55] were used.

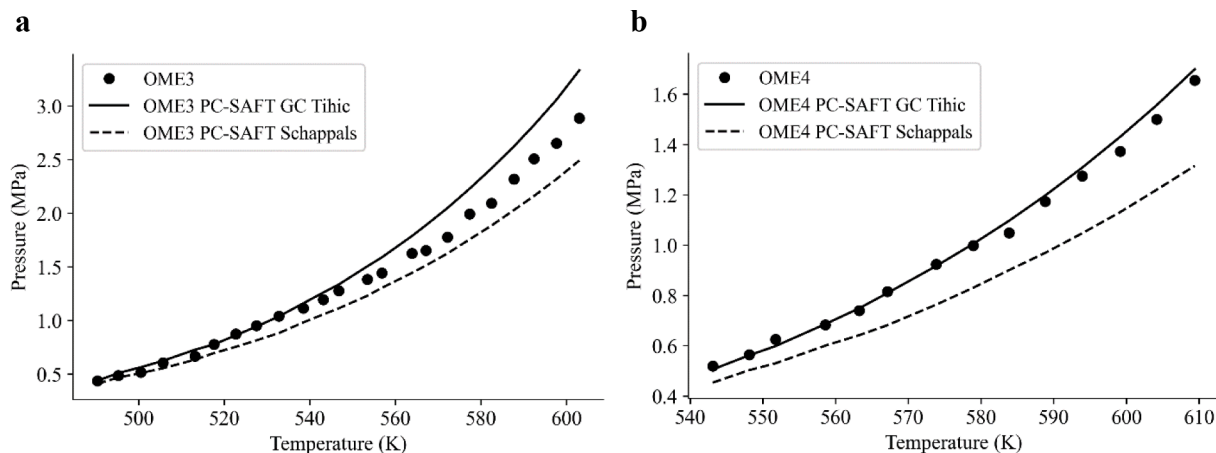


**Fig. 14.** Comparison of PC-SAFT predictions for the vapor pressure, as a function of temperature, of OME<sub>3</sub> and OME<sub>4</sub> against experimental measurements by Fechter et al. [75]. The GC method of Tihic et al. [38] and the parametrization of Schappals et al. [56] were used.

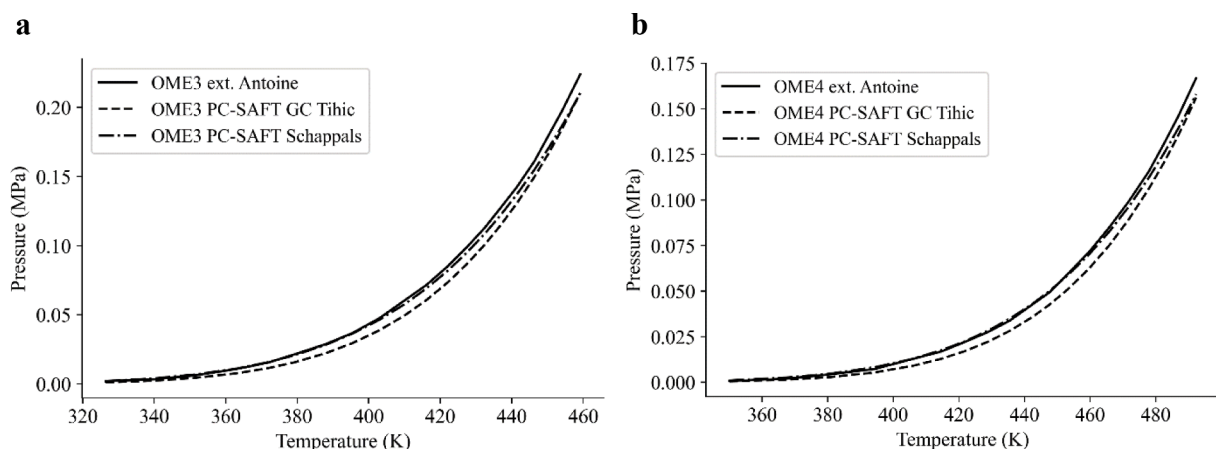


**Fig. 15.** Comparison of PC-SAFT predictions for the vapor pressure, as a function of temperature, of OME<sub>3</sub> and OME<sub>4</sub> against extended Antoine fits by Fechter et al. [75]. The GC method of Tihic et al. [38] and the parametrization of Schappals et al. [56] were used.

OME<sub>4</sub> are compared to the results of the computational model. Like in the previous section, different methods for the estimation of the pure component parameters are employed and the corresponding maximum and average errors are computed. For the C-1 surrogate, the methods of Tihic et al. [38] and Burgess et al. [55] are used, see Fig. 13. Consistent with prior findings, the method of Burgess et al. [55] provides the best match with a maximum error of 37% while the method of Tihic et al. [38] produces an error of up to 57%. The average error using the method of Tihic et al. [38] is 46% and the minimum 33%. In contrast the approach of Burgess et al. [55] yields an average and minimum error of 18% and 7%, respectively.

For OME<sub>3</sub> and OME<sub>4</sub>, we first perform a comparison against the experimental measurements reported by Fechter et al. [75], as shown in Fig. 14. Again, the approaches of Tihic et al. [32] and Schappals et al. [56] are used. The maximum error of the two methods is 25% and 13% for Tihic et al. and Schappals et al., respectively. However, the average error when using the method of Tihic et al. is 8%, while it was 10% with the Schappals et al. method. Since the experimental measurements are limited to temperatures above 490 K, a second investigation is performed at a lower temperature range of 320–460 K using an extended Antoine fit from the work of Fechter et al. [75]. This comparison is presented in Fig. 15. On average, the smallest difference between the results reported by Fechter et al. [75] and this study, about 1%, is achieved by using the parametrization of Schappals et al. [56], proving that it constitutes the most suitable choice.

#### 4. Conclusion

A series of calculations were performed for the distillation curve, density and vapor pressure of various fuel types, namely gasoline, diesel and aviation fuel surrogates with multiple levels of complexity. The study also includes oxygenated fuels: OME and traditional fuel blends with short-chain alcohols. An extensive validation of the thermodynamic model's results was performed by comparing them against the experimental and computational data published elsewhere. The PC-SAFT pure component parameters were calculated using the GC method proposed by Tihic et al. [32], while in some cases the approaches of Burgess et al. [55] and of Schappals et al. [56] were also applied to increase the precision of the results. Overall, there is good agreement between the computational results of the developed model and the data reported in the literature. For the E00 gasoline surrogate, as well as its blends with ethanol and methanol, the results are found to be satisfactory, only with minor deviations at the initial boiling point. The same is true for the PACE surrogates. The diesel/alcohol mixture predictions are not as good, which can be mainly attributed to the modeling of the diesel fuel through the VOb surrogate. The evaporation process of the alcohol in the mixture is predicted successfully in all cases and the results exhibit the same order of precision as the computational data presented by Hernández et al. [72]. In the case of the surrogate for C-1, we conclude that the use of a more advanced GC method published by Burgess et al. [55] can improve the precision of the predicted density

and vapor pressure by up to three times. The use of Schappals et al. [56] parametrization method can also significantly improve the predictions of the model for the OME fuels. These conclusions are expected to some extent, since these above-mentioned models are developed to address flaws of older methodologies and deal with specific fuel types. The results and comparisons presented, demonstrate the predictive capabilities and the generic nature of the developed model, as it has been proven capable of dealing with a large variety of fuel types, while relying only on the chemical composition of each component as input for all computations.

### Declaration of Competing Interest

The authors declare that they have no known competing financial interests or personal relationships that could have appeared to influence the work reported in this paper.

### Data availability

Data will be made available on request.

**Table 4**  
Individual component PC-SAFT input parameters estimated with the method of Tihic et al. [32].

Compound	m	$\sigma$	$\epsilon/k$	$k^{AB}$	$\epsilon^{AB}/k$
n-pentane	2.69	3.77	231.20		
isooctane	3.14	4.09	249.77		
n-undecane	4.91	3.89	248.82		
Isopentane	2.56	3.83	230.75		
Cyclopentane	2.36	3.71	265.83		
Hexene	2.98	3.77	236.81		
Toluene	2.81	3.72	285.69		
heptane	3.48	3.80	238.40		
octadecane	7.44	3.95	254.90		
pentamethyl heptane	3.88	4.25	273.72		
heptamethyl nonane	5.60	4.16	266.46		
1-methylnaphthalene	3.42	3.90	338.79		
Tetralin	3.09	3.99	337.46		
1,2,4-trimethylbenzene	3.61	3.75	284.25		
OME <sub>3</sub>	5.85	3.01	220.84		
OME <sub>4</sub>	7.08	2.98	221.75		
methanol	1.52	3.23	188.90	0.035	2899.50
ethanol	2.38	3.18	198.24	0.032	2653.40
propanol	3.00	3.25	233.4	0.015	2276.80
butanol	2.75	3.61	259.59	0.007	2544.60
pentanol	3.63	3.45	247.28	0.010	2252.10

**Table 5**  
Individual component PC-SAFT input parameters estimated with the method of Burgess et al. [55].

Compound	m	$\sigma$	$\epsilon/k$
pentamethyl heptane	5.25	3.86	224.88
heptamethyl nonane	7.14	3.85	227.96

**Table 6**  
Individual component PC-SAFT input parameters estimated by the method of Schappals et al. [56].

Compound	m	$\sigma$	$\epsilon/k$
OME <sub>3</sub>	4.05	3.55	260
OME <sub>4</sub>	4.83	3.55	260

### Acknowledgements

This project has received funding from the European Union's Horizon 2020 research and innovation program under the Marie Skłodowska-Curie projects No 861002 (EDEM) and No 101028449 (AI-FIE). This Article has been co-authored by National Technology and Engineering Solutions of Sandia, LLC. under contract No. DE-NA0003525 with the U.S. Department of Energy/National Nuclear Security Administration. The United States Government retains and Elsevier, by accepting the article for publication, acknowledges that the United States Government retains a non-exclusive, paid-up, irrevocable, world-wide license to publish or reproduce the published form of this manuscript, or allow others to do so, for United States Government purposes.

### Appendix

## References

- [1] European Expert Group, "Report of the European expert group on future transport fuels," Dusseldorf, Germany, 2011.
- [2] T. Verger, U. Azimov, O. Adeniyi, Biomass-based fuel blends as an alternative for the future heavy-duty transport: A review, *Renewable Sustainable Energy Rev.* 161 (2022), <https://doi.org/10.1016/j.rser.2022.112391>. Jun. 01.
- [3] M. Lapuerta, O. Armas, J. Rodriguez-Fernández, Effect of biodiesel fuels on diesel engine emissions, *Prog. Energy Combust. Sci.* 34 (2) (2008) 198–223, <https://doi.org/10.1016/j.pecs.2007.07.001>.
- [4] S.K. Hoekman, C. Robbins, Review of the effects of biodiesel on NOx emissions, *Fuel Process. Technol.* 96 (2012) 237–249, <https://doi.org/10.1016/j.fuproc.2011.12.036>. Apr.
- [5] J.K. Mwangi, W.J. Lee, Y.C. Chang, C.Y. Chen, L.C. Wang, An overview: Energy saving and pollution reduction by using green fuel blends in diesel engines, *Appl. Energy* 159 (2015) 214–236, <https://doi.org/10.1016/j.apenergy.2015.08.084>. Dec. 01.
- [6] L. Geng, L. Bi, Q. Li, H. Chen, Y. Xie, Experimental study on spray characteristics, combustion stability, and emission performance of a CRDI diesel engine operated with biodiesel–ethanol blends, *Energy Reports* 7 (2021) 904–915, <https://doi.org/10.1016/j.egy.2021.01.043>. Nov.
- [7] A.O. Emiroğlu, M. Şen, Combustion, performance and emission characteristics of various alcohol blends in a single cylinder diesel engine, *Fuel* 212 (2018) 34–40, <https://doi.org/10.1016/j.fuel.2017.10.016>. Jan.
- [8] T. Topgül, H.S. Yücesu, C. Çınar, A. Koca, The effects of ethanol-unleaded gasoline blends and ignition timing on engine performance and exhaust emissions, *Renew. Energy* 31 (15) (2006) 2534–2542, <https://doi.org/10.1016/j.renene.2006.01.004>. Dec.
- [9] S. Iliev, A comparison of ethanol, methanol, and butanol blending with gasoline and its effect on engine performance and emissions using engine simulation, *Processes* 9 (8) (2021), <https://doi.org/10.3390/pr9081322>. Aug.
- [10] I.T. Nazzal, "Experimental Study of Gasoline-Alcohol Blends on Performance of Internal Combustion Engine," 2011. [Online]. Available: <http://www.eurojoournals.com/ejstr.htm>.
- [11] M.E. Tat, J.H. van Gerpen, S. Soyul, M. Canakci, A. Monyem, S. Wormley, Speed of sound and isentropic bulk modulus of biodiesel at 21°C from atmospheric pressure to 35 MPa, *JAOCS, J. Am. Oil Chem. Soc.* 77 (3) (2000) 285–289, <https://doi.org/10.1007/s11746-000-0047-z>.
- [12] M. Wei, S. Li, H. Xiao, G. Guo, Combustion performance and pollutant emissions analysis using diesel/gasoline/iso-butanol blends in a diesel engine, *Energy Convers. Manag.* 149 (2017) 381–391, <https://doi.org/10.1016/j.enconman.2017.07.038>.
- [13] P.K. Koukouvinis, P. Koukouvinis, M. Gavaises, Numerical simulation of cavitation and atomization using a fully compressible three-phase model Numerical simulation of cavitation and atomization using a fully compressible three-phase model Murali-Girija Mithun, *Phys. Rev. Fluids* 00 (2018) 4300, <https://doi.org/10.1103/PhysRevFluids.00.004300>.
- [14] G. Strotos, P. Koukouvinis, A. Theodorakakos, M. Gavaises, G. Bergeles, Transient heating effects in high pressure Diesel injector nozzles, *Int. J. Heat Fluid Flow* 51 (2015) 257–267, <https://doi.org/10.1016/j.ijheatfluidflow.2014.10.010>. Feb.
- [15] A. Theodorakakos, G. Strotos, N. Mitroglou, C. Atkin, M. Gavaises, Friction-induced heating in nozzle hole micro-channels under extreme fuel pressurisation, *Fuel* 123 (2014) 143–150, <https://doi.org/10.1016/j.fuel.2014.01.050>. May.
- [16] A. Vidal, K. Kolovos, M.R. Gold, R.J. Pearson, P. Koukouvinis, M. Gavaises, Preferential cavitation and friction-induced heating of multi-component Diesel fuel surrogates up to 450 MPa, *Int. J. Heat Mass Transf.* 166 (2021), <https://doi.org/10.1016/j.ijheatmasstransfer.2020.120744>. Feb.
- [17] A.J. Rowane, A. Gupta, M. Gavaises, M.A. McHugh, Experimental and modeling investigations of the interfacial tension of three different diesel + nitrogen mixtures at high pressures and temperatures, *Fuel* 280 (2020), <https://doi.org/10.1016/j.fuel.2020.118543>. Nov.
- [18] A.J. Rowane, M. Gavaises, M.A. McHugh, Vapor-liquid equilibria and mixture densities for 2,2,4,4,6,8,8-heptamethylnonane + N<sub>2</sub> and n-hexadecane + N<sub>2</sub> binary mixtures up to 535 K and 135 MPa, *Fluid Phase Equilib.* 506 (2020), <https://doi.org/10.1016/j.fluid.2019.112378>. Feb.
- [19] A.J. Rowane, A. Gupta, M. Gavaises, M.A. McHugh, Experimental and modeling investigations of the phase behavior and densities of diesel + nitrogen mixtures, *Fuel* 265 (2020), <https://doi.org/10.1016/j.fuel.2020.117027>. Apr.
- [20] A.J. Rowane, R.R. Mallepally, M. Gavaises, M.A. McHugh, Interfacial tension of isomers n-hexadecane and 2,2,4,4,6,8,8-heptamethylnonane with nitrogen at high pressures and temperatures, *Ind. Eng. Chem. Res.* 59 (19) (2020) 9293–9299, <https://doi.org/10.1021/acs.iecr.0c00213>. May.
- [21] A.J. Rowane, et al., Effect of Composition, Temperature, and Pressure on the Viscosities and Densities of Three Diesel Fuels, *J. Chem. Eng. Data* 64 (12) (2019) 5529–5547, <https://doi.org/10.1021/acs.jced.9b00652>. Dec.
- [22] A.J. Rowane, R.R. Mallepally, A. Gupta, M. Gavaises, M.A. McHugh, Higherature, High-Pressure Viscosities and Densities of n-Hexadecane, 2,2,4,4,6,8,8-Heptamethylnonane, and Squalene Measured Using a Universal Calibration for a Rolling-Ball Viscometer/Densimeter, *Ind. Eng. Chem. Res.* 58 (10) (2019) 4303–4316, <https://doi.org/10.1021/acs.iecr.8b05952>. Mar.
- [23] G. Strotos, I. Malgarinos, N. Nikolopoulos, M. Gavaises, Predicting the evaporation rate of stationary droplets with the VOF methodology for a wide range of ambient temperature conditions, *Int. J. Therm. Sci.* 109 (2016) 253–262, <https://doi.org/10.1016/j.ijthermalsci.2016.06.022>. Nov.
- [24] C. Rodriguez, H.B. Rokni, P. Koukouvinis, A. Gupta, M. Gavaises, Complex multicomponent real-fluid thermodynamic model for high-pressure Diesel fuel injection, *Fuel* 257 (2019), 115888, <https://doi.org/10.1016/j.fuel.2019.115888> no. February.
- [25] C.J. Mueller, et al., Diesel Surrogate Fuels for Engine Testing and Chemical-Kinetic Modeling: Compositions and Properties, *Energy Fuels* 30 (2) (2016) 1445–1461, <https://doi.org/10.1021/acs.energyfuels.5b02879>. Feb.
- [26] C.J. Mueller, et al., Methodology for formulating diesel surrogate fuels with accurate compositional, ignition-quality, and volatility characteristics, *Energy Fuels* (2012) 3284–3303, <https://doi.org/10.1021/ef300303e>. Jun.
- [27] M.G. Justino Vaz, et al., Numerical Simulation of Multicomponent Diesel Fuel Spray Surrogates Using Real-Fluid Thermodynamic Modelling. SAE Technical Paper Series, SAE International, 2022, <https://doi.org/10.4271/2022-01-0509>. Mar.
- [28] J. Hwang, et al., Machine-learning enabled prediction of 3D spray under engine combustion network spray G conditions, *Fuel* 293 (2021), <https://doi.org/10.1016/j.fuel.2021.120444>. Jun.
- [29] A. Tihic, G.M. Kontogeorgis, N. von Solms, M.L. Michelsen, Applications of the simplified perturbed-chain SAFT equation of state using an extended parameter table, *Fluid Phase Equilib.* 248 (1) (2006) 29–43, <https://doi.org/10.1016/j.fluid.2006.07.006>. Oct.
- [30] F. Tumakaka, G. Sadowski, Application of the Perturbed-Chain SAFT equation of state to polar systems, *Fluid Phase Equilib.* 217 (2) (2004) 233–239, <https://doi.org/10.1016/j.fluid.2002.12.002>. Mar.
- [31] F. Tumakaka, J. Gross, G. Sadowski, Thermodynamic modeling of complex systems using PC-SAFT, *Fluid Phase Equilib.* 228–229 (2005) 89–98, <https://doi.org/10.1016/j.fluid.2004.09.037>. Feb.
- [32] S. Leekunjom, K. Krejbjerg, Phase behavior of reservoir fluids: Comparisons of PC-SAFT and cubic EOS simulations, *Fluid Phase Equilib.* 359 (2013) 17–23, <https://doi.org/10.1016/j.fluid.2013.07.007>. Dec.
- [33] J. Gross, G. Sadowski, Perturbed-Chain SAFT : An Equation of State Based on a Perturbation Theory for Chain Molecules, *Ind. Eng. Chem. Res.* 40 (2001) 1244–1260.
- [34] M. Hopp, J. Gross, Thermal Conductivity from Entropy Scaling: A Group-Contribution Method, *Ind. Eng. Chem. Res.* 58 (44) (2019) 20441–20449, <https://doi.org/10.1021/acs.iecr.9b04289>.
- [35] L. Oliver and J. Gross, "A group contribution method for viscosities based on entropy scaling using the perturbed-chain polar statistical associating fluid theory," pp. 1–28, 1977.
- [36] M. Hopp and J. Gross, "Thermal Conductivity of Real Substances from Excess Entropy Scaling Using PC-SAFT," 2017, doi: 10.1021/acs.iecr.6b04289.
- [37] E. Sauer, M. Stavrou, J. Gross, Comparison between a homo- and a heterosegmented group contribution approach based on the perturbed-chain polar statistical associating fluid theory equation of state, *Ind. Eng. Chem. Res.* 53 (38) (2014) 14854–14864, <https://doi.org/10.1021/ie502203w>. Sep.
- [38] A. Tihic, G.M. Kontogeorgis, N. Von Solms, M.L. Michelsen, A predictive group-contribution simplified PC-SAFT equation of state: Application to polymer systems, *Ind. Eng. Chem. Res.* 47 (15) (2008) 5092–5101, <https://doi.org/10.1021/ie0710768>. Aug.
- [39] J. Gross and M. Stavrou, "Fluid Phase Equilibria Estimation of the binary interaction parameter  $k_{ij}$  of the PC-SAFT Equation of State based on pure component parameters using a QSPR method," vol. 416, pp. 138–149, 2016, doi: 10.1016/j.fluid.2015.12.016.
- [40] J. Gross, G. Sadowski, Application of the perturbed-chain SAFT equation of state to associating systems, *Ind. Eng. Chem. Res.* 41 (22) (2002) 5510–5515, <https://doi.org/10.1021/ie010954d>.
- [41] P. Koukouvinis, C. Rodriguez, J. Hwang, I. Karathanassis, M. Gavaises, L. Pickett, Machine Learning and transcritical sprays: A demonstration study of their potential in ECN Spray-A, *Int. J. Engine Res.* 23 (9) (2022) 1556–1572, <https://doi.org/10.1177/14680874211020292>. Sep.
- [42] A. Vidal, P. Koukouvinis, M. Gavaises, Vapor-liquid equilibrium calculations at specified composition, density and temperature with the perturbed chain statistical associating fluid theory (PC-SAFT) equation of state, *Fluid Phase Equilib.* 521 (2020), <https://doi.org/10.1016/j.fluid.2020.112661>. Oct.
- [43] P. Koukouvinis, A. Vidal-Roncero, C. Rodriguez, M. Gavaises, and L. Pickett, "Enhancing the predictive capabilities for high P/T fuel sprays; non-ideal thermodynamic modelling using PC-SAFT," Nov. 2020, [Online]. Available: <http://arxiv.org/abs/2011.09983>.
- [44] C. Rodriguez, P. Koukouvinis, M. Gavaises, Simulation of supercritical diesel jets using the PC-SAFT EoS, *J. Supercrit. Fluids* 145 (November 2018) (2019) 48–65, <https://doi.org/10.1016/j.supflu.2018.11.003>.
- [45] A. Vidal, C. Rodriguez, P. Koukouvinis, M. Gavaises, M.A. McHugh, Modelling of Diesel fuel properties through its surrogates using Perturbed-Chain, Statistical Associating Fluid Theory, *Int. J. Engine Res.* 21 (7) (2020) 1118–1133, <https://doi.org/10.1177/1468087418801712>. Sep.
- [46] D.Y. Peng, D.B. Robinson, A New Two-Constant Equation of State, *Ind. Eng. Chem. Fundam.* 15 (1) (1976) 59–64, <https://doi.org/10.1021/i160057a011>.
- [47] G. Soave, Equilibrium constants from a modified Redlich-Kwong equation of state, *Chem. Eng. Sci.* 27 (6) (1972) 1197–1203, [https://doi.org/10.1016/0009-2509\(72\)80096-4](https://doi.org/10.1016/0009-2509(72)80096-4).
- [48] P. Koukouvinis, A. Vidal-Roncero, C. Rodriguez, M. Gavaises, L. Pickett, High pressure/high temperature multiphase simulations of dodecane injection to nitrogen: Application on ECN Spray-A, *Fuel* 275 (2020), 117871, <https://doi.org/10.1016/j.fuel.2020.117871> no. February.
- [49] S. Stamataki, Performance of cubic eos at high pressures, *Revue de l'Institut Français du Pétrole* 53 (3) (1998) 367–376, <https://doi.org/10.2516/ogst:1998032>.

- [50] B.M. Ningeowda, F.N.Z. Rahantamalisoa, A. Pandal, H. Jasak, H.G. Im, M. Battistoni, Numerical modeling of transcritical and supercritical fuel injections using a multi-component two-phase flow model, *Energies (Basel)* 13 (21) (2020), <https://doi.org/10.3390/en13215676>. Nov.
- [51] K. Kolovos, N. Kyriazis, P. Koukouvunis, A. Vidal, M. Gavaises, R.M. McDavid, Simulation of transient effects in a fuel injector nozzle using real-fluid thermodynamic closure, *Appl. Energ. Combust. Sci.* 7 (2021), 100037, <https://doi.org/10.1016/j.jaecs.2021.100037>. Sep.
- [52] W.G. Chapman, K.E. Gubbins, G. Jackson, and M. Radosz, "New Reference Equation of State for Associating Liquids," pp. 1709–1721, 1990.
- [53] S.H. Huang and M. Radosz, "Equation of State for Small, Large, Polydisperse, and Associating Molecules," pp. 2284–2294, 1990, doi: 10.1021/ie00107a014.
- [54] S.H. Huang and M. Radosz, "Equation of State for Small, Large, Polydisperse, and Associating Molecules : Extension to Fluid Mixtures," pp. 1994–2005, 2005.
- [55] W.A. Burgess, D. Tapriyal, I.K. Gamwo, Y. Wu, M.A. McHugh, R.M. Enick, New group-contribution parameters for the calculation of PC-SAFT parameters for use at pressures to 276 MPa and temperatures to 533 K, *Ind. Eng. Chem. Res.* 53 (6) (2014) 2520–2528, <https://doi.org/10.1021/ie4034973>. Feb.
- [56] M. Schappals, T. Breug-Nissen, K. Langenbach, J. Burger, H. Hasse, Solubility of Carbon Dioxide in Poly(oxyethylene) Dimethyl Ethers, *J. Chem. Eng. Data* 62 (11) (2017) 4027–4031, <https://doi.org/10.1021/acs.jced.7b00718>. Nov.
- [57] M.L. Michelsen, J.M. Mollerup, *Thermodynamic models : Fundamentals & Computational Aspects*, Tie-Line Publications, 2007.
- [58] G.M. Wilson, A modified Redlich-Kwong equation of state, application to general physical data calculations, in: 65th National AIChE Meeting, Cleveland, 1969.
- [59] M. Michelsen, The isothermal flash problem, *Fluid Phase Equilib.* (9) (1982) 1–19.
- [60] J. Mikyška, A. Firoozabadi, Investigation of mixture stability at given volume, temperature, and number of moles, *Fluid Phase Equilib.* 321 (May 2012) 1–9, <https://doi.org/10.1016/j.fluid.2012.01.026>.
- [61] J. Nocedal, S. Wright, *Numerical Optimization*, Springer, New York, 2006.
- [62] R. Fletcher, *Practical Methods of Optimization*, John Wiley & Sons, 2013.
- [63] R.B. Schnabel, E. Eskow, and S.J. Optim, "A revised modified Cholesky factorization algorithm \*." [Online]. Available: <http://www.siam.org/journals/iopt/9-4/33266.html>.
- [64] J.T. Edwards, Reference Jet Fuels for Combustion Testing, in: 55th AIAA Aerospace Sciences Meeting, Reston, Virginia, American Institute of Aeronautics and Astronautics, Jan. 2017, <https://doi.org/10.2514/6.2017-0146>.
- [65] J.M. Desantes, J.V. Pastor, J.M. García-Oliver, J.M. Pastor, A 1D model for the description of mixing-controlled reacting diesel sprays, *Combust. Flame* 156 (1) (2009) 234–249, <https://doi.org/10.1016/j.combustflame.2008.10.008>. Jan.
- [66] R. Fang, et al., Fuel molecular structure effect on autoignition of highly branched iso-alkanes at low-to-intermediate temperatures: Iso-octane versus iso-dodecane, *Combust. Flame* 214 (2020) 152–166, <https://doi.org/10.1016/j.combustflame.2019.12.037>. Apr.
- [67] *ASTM D86 Standard Test Method for Distillation of Petroleum Products At Atmospheric Pressure, D86-10*, ASTM International, West Conshohocken, 2010.
- [68] R.L. McCormick, et al., Co-Optimization of Fuels & Engines: Properties of Co-Optima Core Research Gasolines, Golden, CO (United States), 2018, <https://doi.org/10.2172/1467176>. Aug.
- [69] V.F. Andersen, J.E. Anderson, T.J. Wallington, S.A. Mueller, O.J. Nielsen, Distillation Curves for Alcohol–Gasoline Blends, *Energy Fuels* 24 (4) (2010) 2683–2691, <https://doi.org/10.1021/ef9014795>. Apr.
- [70] I.K. Karathanassis, L. White, P. Koukouvunis, J. Hwang, L. Pickett, and M. Gavaises, "Comparative Investigation of Gasoline-like Surrogate Fuels using 3D Computed Tomography," 2021.
- [71] S. Cheng, et al., Replicating HCII-like autoignition behavior: What gasoline surrogate fidelity is needed? *Appl. Energ. Combust. Sci.* 12 (2022), 100091 <https://doi.org/10.1016/j.jaecs.2022.100091>. Dec.
- [72] J.P. Hernández, F. Bustamante, J.R. Agudelo, Thermodynamics of semicontinuous n-alcohol/ultra-low sulfur diesel blends, *Fluid Phase Equilib.* 401 (2015) 9–15, <https://doi.org/10.1016/j.fluid.2015.05.013>. Sep.
- [73] M. Colket, et al., Overview of the National Jet Fuels Combustion Program, *AIAA J.* 55 (4) (2017) 1087–1104, <https://doi.org/10.2514/1.J055361>. Apr.
- [74] H. Wu, P.C. Ma, T. Jaravel, M. Ihme, Application of pareto-efficient combustion modeling framework to large eddy simulations of turbulent reacting flows, in: *AIAA Aerospace Sciences Meeting*, American Institute of Aeronautics and Astronautics Inc, AIAA, 2018, <https://doi.org/10.2514/6.2018-1667>, 2018.
- [75] M.H.H. Fechter, P. Haspel, C. Hasse, A.S. Braeuer, Vapor pressures and latent heats of vaporization of Poly(oxyethylene) Dimethyl Ethers (OME3 and OME4) up to the vicinity of the critical temperature, *Fuel* 303 (2021), <https://doi.org/10.1016/j.fuel.2021.121274>. Nov.
- [76] A. Kulkarni, et al., A Force Field for Poly(oxyethylene) Dimethyl Ethers (OME n), *J. Chem. Theor. Comput.* 16 (4) (2020) 2517–2528, <https://doi.org/10.1021/acs.jctc.9b01106>. Apr.